Enhanced removal of phosphate from water by fabricating a novel dual metal MIL-101(Fe/Zr)

JIAO Zhen[1,2,4,5] ,MIAO Zhijia[2,3,4,5] ,LI Qing[2,3] ,
AN Heluan[2,3] ,MENG Xiangyuan[2,3] ,SONG Cunyi[1]

(1. School of Energy and Environmental Engineering ,University of Science and Technology Beijing ,Beijing 100083,China.
2. School of Water Resources and Environment , Hebei GEO University , Shijiazhuang 050031,China. 3. Hebei Provincial
Laboratory of Water Environment Science , Hebei Provincial Academy of Ecological Environmental Science , Shijiazhuang
050031,China. 4. Hebei Province Collaborative Innovation Center for Sustainable Utilization of Water Resources and
Optimization of Industrial Structure , Hebei GEO University , Shijiazhuang 050031,China. 5. Hebei Center for Ecological
and Environmental Geology Research , Hebei GEO University , Shijiazhuang 050031,China)

Abstract:Metal-based compounds are promising adsorbents for phosphate. A novel dual metal-organic framework as an effective adsorbent for phosphate was synthesized by a solvothermal method. The structure analysis revealed that the as-prepared adsorbent (denoted as MIL-101(Fe/Zr)) possessed a porous polyhedral structure with a large specific surface area of 479.1 m^2/g and a pore width of 3.4 nm. The X-ray diffraction pattern and Fourier transform infrared spectra suggested that the MIL-101(Fe/Zr) shared a similar structure with MIL-101(Fe),implying successful incorporation of Zr atoms as a second metal into the MIL-101(Fe) structure. Kinetic adsorption of PO_4^{3-} by MIL-101(Fe/Zr) conformed to the pseudo-second-order model and intraparticle diffusion model,while adsorption isotherm fitted the Freundlich model well ($R^2=0.978\ 5$). It is suggested that such an adsorption belonged to multiply-layer adsorption. The adsorption capacity of MIL-101(Fe/Zr) was to be 66.00 mg/g. MIL-101(Fe/Zr) performed well at a wide range of pH 2.0~10.0 and high ionic strength (0~40 mg/L NaCl). A structural analysis indicated that the complexation interaction was mainly responsible for PO_4^{3-} adsorption. These findings can inspire preparation of other dual metal MOFs adsorbent for phosphate removal and recovery from water.

Key words:MOF_s ;MIL-101(Fe);adsorption;phosphate;complexation interaction

Chinese Library Classification No.:TV213　　**Document Code**:A　　OSID:

1　Introduction

Phosphorus provides an essential nutrient for the growth of living life in aquatic ecosystem[1-2]. When the environment accommodates excessive phosphate from agricultural runoff or industrial

discharges, it would give rise in a eutrophication and thus deterioration of water quality[3]. Noticeably, it also brings a big challenge to the survival of many aquatic life and the safety of drinking water supply[4-5]. It is evaluated that a trace amount of phosphate (above 0.02 mg/L) is able to induce undesirable eutrophication. Therefore, removal of phosphate from water will be of great significance to prevent eutrophication[3].

There have been reported a lot of methods for controlling phosphate, such as chemical methods, physical methods, and biological methods[6-7]. Among them, the chemical methods aroused an extensive attention due to simple operation, low cost, and high efficiency[5,8]. Adsorption, as a traditional method, plays an important role in removal of phosphate from water. Generally, adsorptive performance relied greatly on the structure and properties of adsorbents[9-10]. Thus, development of novel and excellent adsorbents with fast adsorption kinetics and high adsorption capacity was always a big challenge. Up to date, many adsorbents to enhance phosphate elimination from aquatic environment have been reported by searchers[11]. These could be roughly categorized into several types: carbonaceous materials, mineral substance, biomass-derived materials, and other novel synthetic materials[12-13].

Particularly, metal-organic frameworks (MOFs), built from inorganic metal nodes bridged with organic ligands, emerging as novel and porous materials have drawn a lot of attentions[14-16]. Such materials possess uniformly ordered pore size, large specific surface area, and good chemical stability[17-18]. Recently, MOFs have been demonstrated as excellent adsorbents for phosphate[19-21]. For instance, a cerium-doped MIL-101-NH$_2$(Fe) was reported as superior adsorbent for simultaneous removal of phosphate and arsenate[22]. Roles of defects and linker exchange in phosphate adsorption on UiO-66 type metal organic frameworks were also investigated[23]. Another MOF-based heterostructure was developed to enhance phosphate removal from practical wastewater via a in situ engineered strategy[24]. These suggested that MOFs have great promise in recovery and removal of phosphate from water, and meanwhile that adsorption performance of MOFs depends significantly on their structures and components[25]. It is supposed that metal species (nodes of MOFs) may play important roles in adsorption of phosphate due to a high electronegative property of phosphate, and their strong coordination interactions with Lewis acid[26].

Encouraged by previous literature, we assumed that introduction of a second metal into the classical MOFs may create a different topology structure, and thus bring some unique interfacial properties. This would be beneficial to phosphate adsorption. However, the relationship between the MOF structure formed by doped metal and adsorption property is still unclear. A novel dual metal-organic framework (MIL-101(Fe/Zr)) was synthesized by a solvothermal method. Its structure was characterized and pore properties were analyzed. Adsorption kinetics and isotherms of MIL-101(Fe/Zr) as well as effects of initial solution pH and ionic strength on adsorption of phosphate were fully investigated. The phosphate adsorption mechanisms were demonstrated by a microstructure analysis of MIL-101 (Fe/Zr) before and after adsorption.

2 Experimental section

2.1 Materials and reagents

Ferric chloride hexahydrate (FeCl$_3$ · 6H$_2$O), zirconium chloride (ZrCl$_4$), sodium chloride (NaCl), sodium hydroxide (NaOH), concentrated hydrochloric acid (HCl, 36%~38%) and terephthalic acid (H$_2$BDC) were purchased from Sinopharm Chemical Reagent Co., Ltd (Shanghai, China). N, N-dimethylformamide (DMF) was obtained from Aladdin reagent company (USA). All reagents were of analytical grade, and used directly when received. Phosphate stock solution was prepared by dissolving KH$_2$PO$_4$ in deionized water. Deionized water with the conductivity of 18.2 MΩ/cm (DIW) was prepared by the water purification device (Kertone Water Treatment Co., Ltd, China).

2. 2　Synthesis of MIL-101(Fe/Zr),MIL-101(Fe) and UiO-66

Typically, 0. 664 4 g of H_2BDC, 0. 810 6 g of $FeCl_3 \cdot 6H_2O$, and 0. 233 0 g of $ZrCl"4$ were dissolved in 80 mL DMF. And then the mixture in a Teflon-lined stainless-steel autoclave (100 mL) was transferred to an electric oven to react at 150 ℃ for 15 h. After reaction, the precipitate was collected by centrifugation and washed by absolute ethanol and ultrapure water repeatedly. Finally, the product was dried overnight at 80 ℃ for further use. The product was denoted as MIL-101(Fe/Zr).

For comparison, either $FeCl_3 \cdot 6H_2O$ or $ZrCl_4$ were added into the mixture to produce MIL-101 (Fe) or UiO-66(Zr). Unless specific statement, other reaction conditions were kept the same to synthesis of MIL-101(Fe/Zr).

2. 3　Materials Characterization

The microstructure and surface elements of the as-prepared adsorbents were observed on a Hitachi SU-8010 field emission scanning electron microscope (FESEM) equipped with an energy dispersive X-ray detector (EDX). Transmission electron microscope (TEM) images were observed on a Hitachi-7700 electron microscope. Powder X-ray diffraction (PXRD) patterns were recorded on an X′Pert PRO diffractor with monochromatized K_α radiation ($\lambda = 0. 154$ nm). Fourier transform infrared spectra (FT-IR) were collected on a Thermo Fisher Scientific Nicolet 6700 instrument. X-ray photoelectron spectroscopy (XPS) was measured on a PHI 5000C ESCA spectrometer with a monochromatized Al K_α source. The peaks were fitted using XPSPEAK41 software and the binding energy was corrected by a reference (284. 5 eV of C 1s). Nitrogen adsorption-desorption isotherm was performed on a Quanta chrome Autosorb-1 chemisorption apparatus at 77 K.

2. 4　Adsorption experiments

Adsorption experiments were conducted in a batch mode. The adsorption kinetics were determined by adding 5 mg adsorbent into 10 mL solution with initial mass concentrations of phosphate (PO_4^{3-}) (5 mg/L). At predetermined time intervals, aliquots were withdrawn and filtered. Similarly, the adsorption isotherm experiments were performed in the mass concentration range of 5. 0 ~ 50. 0 mg/L. The adsorption experiments were allowed to proceed in a shaker (25 ℃) for 24 h to assure an adsorption equilibrium.

The effect of solution pH on adsorption was examined within pH of 2. 0 ~ 10. 0 (The solution pH was adjusted by HCl or NaOH solution). The ionic strength tests were investigated by separately adding ions (NaCl) into phosphate solution (50. 0 mg/L). The NaCl mass concentrations were approximately 10, 20, 30 and 40 mg/L, respectively. After adsorption, a small portion of sample solutions were withdrawn and filtered through 0. 22 μm syringe filters, and analyzed by an ammonium molybdate spectrophotometric method at the wavelength of 700 nm on a UV-1780 spectrophotometer (Shimadzu Corporation, Japan) and reported as PO_4^{3-}. Adsorption experiments were performed in duplicate and reported by average values. The removal efficiency (R, %), and adsorption amount (q_t, mg/g) were calculated from Equations (1) and (2):

$$R = \frac{(C_0 - C_e)}{C_0} \times 100\% \qquad (1)$$

$$q_t = \frac{(C_0 - C_t) \times V}{m} \qquad (2)$$

Where C_0, C_t and C_e, mg/L are the initial mass concentration, the instant mass concentration at time t and the equilibrium concentration of phosphate in the solution, respectively. V, mL represents the volume of the phosphate solution, and m, g the mass of the adsorbent.

3　Results and discussion

3. 1　Structural analysis of MIL-101(Fe/Zr)

As shown in Fig. 1, MIL-101(Fe), UiO-66, and MIL-101(Fe/Zr) possessed polyhedral structure, but they shared different morphology. MIL-101 (Fe) showed irregular tetrahedrons while UiO-66 was of irregular octahedrons. Interestingly, MIL-101 (Fe/Zr) exhibited a more similar structure to MIL-101 (Fe) than those of UiO-66. This could be explained by that the formation of MIL-101(Fe) was dominated in the coordination process and zirconium atoms were doped into the former due to a small content. In

spite of zirconium atoms in a small quantity, the stronger coordination tendency made themselves successfully

dope into MIL-101(Fe) structure, thus forming a dual metal-organic framework.

(a) MIL-101　　　(b) Vio-66　　　(c) MIL-101(Fe/Zr)　　　(d) MIL-101(Fe/Zr)
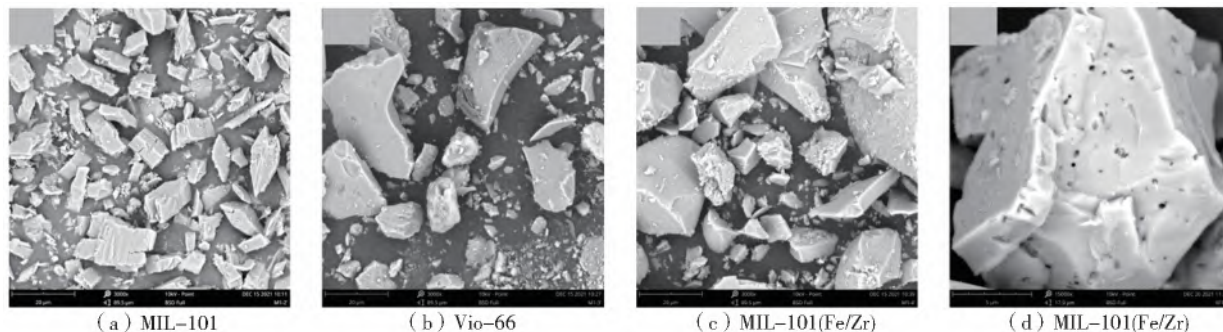
Fig. 1　SEM images of MIL-101, UiO-66, fresh MIL-101(Fe/Zr) and used MIL-101(Fe/Zr)

FT-IR spectra provide another evidence for MIL-101(Fe/Zr) formation. As shown in Fig. 2, the spectrum of MIL-101(Fe/Zr) exhibited a similar character with MIL-101(Zr). A peak located at 500 cm^{-1} could be assigned to the stretching vibration of Fe-O, while one located at 800 cm^{-1} should be the stretching vibration of Zr-O. Those peaks were across 1 200 cm^{-1} to 2 000 cm^{-1} in three samples, suggesting the characteristic zone of benzene ring. These facts strongly proved a dual metal-organic framework was successfully formed under current synthetic conditions.
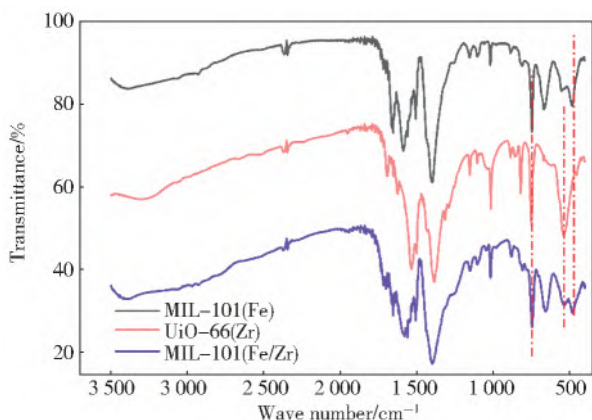
Fig. 2　FT-IR spectra of MIL-101(Fe), UiO-66(Zr), and MIL-101(Fe/Zr)

PXRD patterns of MIL-101(Fe), UiO-66(Zr), and MIL-101(Fe/Zr) are displayed in Fig. 3. Obviously, MIL-101(Fe/Zr) showed identical patterns with MIL-101(Fe) but it was very different from that of UiO-66. For instance, a typical peak at $2\theta=$ 7.3° belonged to MIL-101, whereas the peak at $2\theta=12.5°$ may originate from UiO-66. As for MIL-101(Fe/Zr), it showed a diffraction peak at $2\theta=$ 7.3°, which suggested MIL-101 (Fe/Zr) shared same topology structure with MIL-101(Fe). This fact was consistent with SEM observation and FT-

IR analysis, strongly evidencing the formation of MIL-101(Fe/Zr).
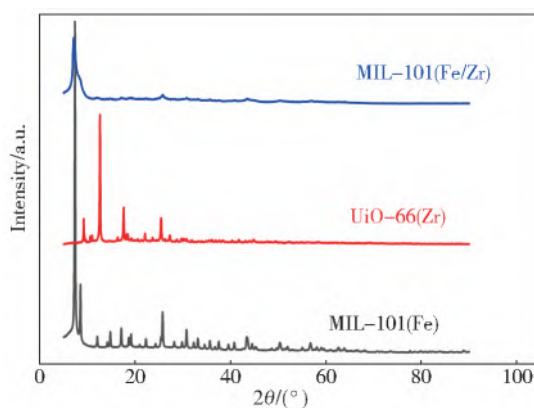
Fig. 3　XRD patterns of MIL-101(Fe), UiO-66(Zr), and MIL-101(Fe/Zr)

XPS can offer some important information of surface elements of materials. As shown in Fig. 4, it can be easily found carbon, oxygen, iron, and zirconium elements in spectrum of MIL-101 (Fe/Zr). This observation indicated zirconium atoms were introduced into the MOF structure, forming a new dual-metal organic framework. After adsorption, the peak of phosphorus looked remarkable, which further suggested that phosphate had been attached to the surface of MIL-101(Fe/Zr).
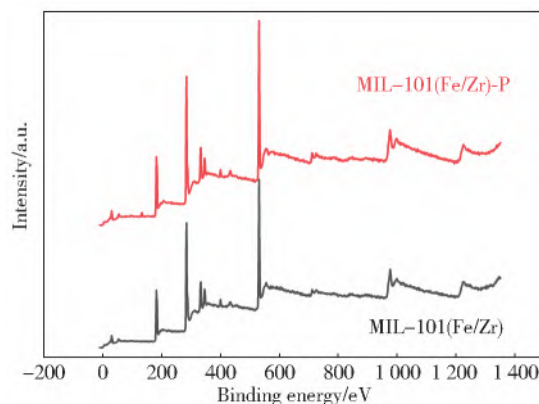
Fig. 4　XPS spectra of MIL-101(Fe/Zr) before and after adsorption

The N_2 adsorption-desorption isotherm and pore size distribution are shown in Fig. 5. Clearly, the isotherm belonged to a typical type II isotherm with a H3 hysteresis,implying that the structure of MIL-101(Fe/Zr) had mesoporous pores,and this would facilitate diffusion and adsorption of pollutants. As shown in Fig. 5(b),the Brunauer-Emmett-Teller (BET) specific surface area is to be 479. 13 m^2/g. Calculated from the Barrett-Joyner-Halenda (BJH) model (the desorption branch),the pore size and pore volume is to be 3. 412 nm and 0. 183 cm^3/g. This mesoporous structure may be beneficial for adsorption.
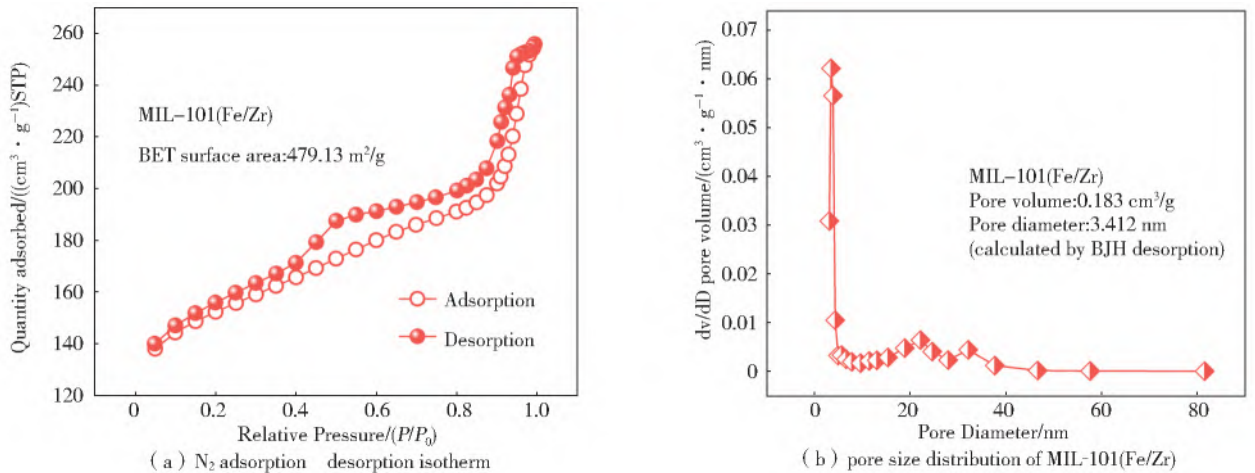
Fig. 5　N_2 adsorption-desorption isotherm and pore size distribution of MIL-101(Fe/Zr)

3. 2　Adsorption performance of MIL-101 (Fe/Zr)

3. 2. 1　Adsorption kinetics

The effects of contact time on instantaneous concentration of PO_4^{3-} is shown in Fig. 6(a). As the contact time of t (h) prolonged,the PO_4^{3-} concentration dropped dramatically at initial stage and then reached a platform,no matter in UiO-66(Zr) or MIL-101 (Fe/Zr) system. Noticeably, the dropped degree of mass concentrations was different. For UiO-66 (Zr), the mass concentration changed from 10. 10 to 6. 98 mg/L. However,the mass concentration dropped instantly to 2. 08 from 10. 10 mg/L for MIL-101(Fe/Zr). It is obvious that MIL-101 (Fe/Zr) showed an enhanced adsorption performance comparing to UiO-66(Zr). This may be because doping of a second metal creates unique structure and some defects of MIL-101 (Fe/Zr), which facilitated removal and recovery of PO_4^{3-}.

For evaluation of adsorption kinetics,the pseudo-first-order model (PFO), the pseudo-second-order model (PSO),and the intraparticle diffusion model (IPD) were used to fit experimental data. The equations of adsorption kinetics are provided as follows[27-28]:

Pseudo first-order model
$$\ln(q_e-q_t)=\ln q_e-k_1 t \tag{3}$$
Pseudo second-order model
$$\frac{t}{q_t}=\frac{1}{k_2 q_e^2}+\frac{1}{q_e}t \tag{4}$$
Intra-particle diffusion model
$$q_t=k_i t^{0.5}+C_i \tag{5}$$
Where q_t and q_e,mg/g in Eqs. (3) and (4) represent the instantaneous adsorption amount of phosphate (t) and the equilibrium adsorption amount of phosphate (equilibrium time). C_i,mg/g in Eq. (5) depicts the effect of boundary layer. $k_1 (\text{min}^{-1})$,k_2 $[g/(mg \cdot \text{min})^{-1}]$ and $k_i[mg/(g \cdot \text{min}^{-0.5})^{-1}]$ are the rate constants of pseudo first-order, pseudo second-order and intraparticle diffusion in Eqs (3)、(4) and (5),respectively.

The fitting curves and results are displayed in Fig. 6(b-d). The correlation coefficients (R^2) of PSO (0. 997 8) and IPD (0. 986 7 and 0. 985 8 of the two stage) were similar to that of PFO (0. 996 8). Moreover,the q_e of PSD (16. 10 mg/g) was much closer to the experimental value (16. 06 mg/g) than that of PFO (13. 86 mg/g) and IPD (7. 30 mg/g). It can easily be found that PSO fitted better for kinetic data than PFO and IPD. This

demonstrated that the adsorption process was jointly controlled by chemisorption and diffusion mechanism, which may be determined by the unique structure of MIL-101(Fe/Zr)[29].

(a) UiO-66(Zr),and MIL-101(Fe/Zr)

(b) Pseudo first-order model

(c) Pseudo second-order model

(d) Intraparticle diffusion model
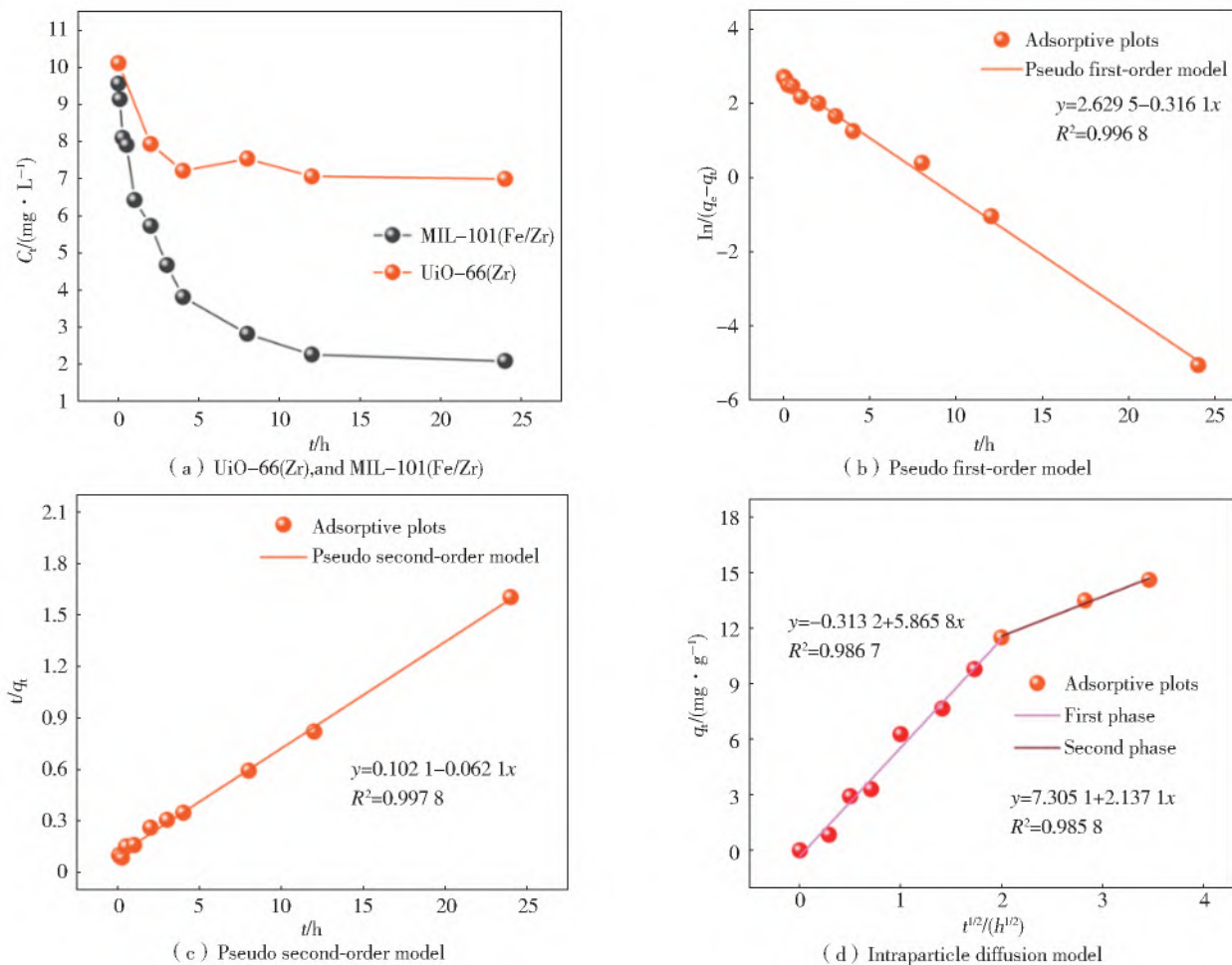
Fig. 6   ffect of contact time on concentration of PO_4^{3-} treated by

Tab. 1   Kinetics parameters of three kinetic models

Pseudo first-order model			Pseudo second-order model			Intraparticle-diffusion model		
R^2	q_e(mg $\cdot$ g^{-1})	k_1/h^{-1}	R^2	q_e/(mg $\cdot$ g^{-1})	k_2/(g $\cdot$ (mg $\cdot$ min^{-1})	R^2	C_i(mg $\cdot$ g^{-1})	k_{id}/(mg $\cdot$ g^{-1} $\cdot$ t$^{1/2}$)
0. 996 8	13. 86	0. 316 1	0. 997 8	16. 10	0. 037 8	0. 986 7	0	5. 865 8
						0. 985 8	7. 305 1	2. 137 1

3.2.2   Adsorption isotherm

The adsorption isotherm of phosphate by MIL-101(Fe/Zr) was analyzed by the Langmuir model, and Freundlich model (Fig. 7). The fitting parameters are shown in Tab. 2. As for the isotherm process, the adsorption amount gradually increased when the initial mass concentration increased. When the active sites were completely occupied by phosphate, a saturation adsorption platform can be achieved. According to the R^2 (0. 978 5), it is obvious that the Freundlich model can fit best for adsorption, indicating this adsorption was a multi-layer heterogeneous adsorption[30]. The un-

satisfactory R^2 suggested the adsorption did not comfort to the Langmuir model ($R^2 = 0.881\ 4$). Calculated from the Langmuir model, the theoretically maximum adsorption capacity of MIL-101 (Fe/Zr) (q_m) was to be 66. 00 mg/g.

Equations of adsorption isotherms[31]

$$q_e = \frac{K_L q_m C_e}{1 + K_L C_e} \tag{6}$$

$$q_e = K_F C_e^{\frac{1}{n}} \tag{7}$$

Where C_e, mg/L and q_e, mg/g are the equilibrium concentration of phosphate and its corresponding equilibrium adsorption capacity, respectively. K_L, L/mg and K_F, mg/g (L/mg)$^{1/n}$ represent the con-

stant of the Langmuir model and Freundlich model，respectively.
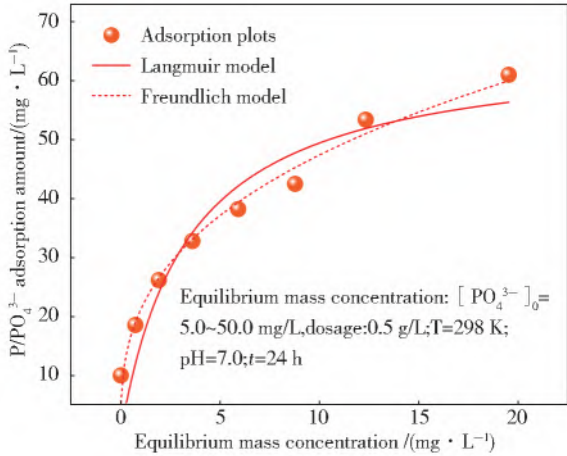
Fig. 7 Adsorptive isotherm of MIL-101(Fe/Zr)

Tab. 2 Isotherm parameters of two isothermal models

Langmuir model			Freundlich model		
R^2	$q_m/$ (mg•g^{-1})	$K_L/$ (L•mg^{-1})	R^2	n	$K_F/$ (mg•g^{-1})(L•mg^{-1})$^{1/n}$
0. 881 4	66. 00	0. 30	0. 978 5	2. 84	21. 03

A comparison among recently reported adsorbents was made，as listed in Tab. 3. Their adsorption capacity of PO_4^{3-} is among 16. 14～64. 52 mg/g. The as-prepared MIL-101(Fe/Zr) displayed a comparable adsorption capacity (66. 00 mg/g) to most of adsorbents listed[28,32]. Considering the simple preparation and convenient separation，MIL-101 (Fe/Zr) may be a potential adsorbent for phosphate removal.

Tab. 3 Comparison of PO_4^{3-} adsorption capacity of newly reported adsorbents

Adsorbents	Mass concentration/ (mg•L^{-1})	Maximum capacity/ (mg•g^{-1})	Refs
CDC	1. 0～100	16. 14	[32]
UiO-66	9. 6～192. 0	48. 96	[23]
PS-M-LDH	5. 0～50	34. 20	[33]
Cry-CSH	0. 1～100	64. 52	[28]
MIL-101(Fe/Zr)	5. 0～50. 0	66. 00	This study

3. 2. 3 Effects of initial solution pH and ionic strength

The effect of initial solution pH on adsorption amount is shown in Fig. 8(a). When pH ranging from 2. 0 to 10. 0，the adsorptive amount (q_e) dropped to 53. 3 from 73. 9 mg/g. As pH increased to 10. 0，q_e underwent a moderate decline to 53. 3 mg/g. In weak acid system，the protons showed no obvious competitive influence on MIL-101(Fe/Zr). However，in an alkaline system，the reason of decreased adsorption activity was probably due to the reduction of active sites. As previously reported，plenty of OH-may induce degradation of a fraction of MIL-101(Fe/Zr)[33]. Totally，MIL-101(Fe/Zr) exhibited an excellent removal performance towards phosphate in an acidic solution，however，it was not favored in a neutral or an alkaline condition[34].
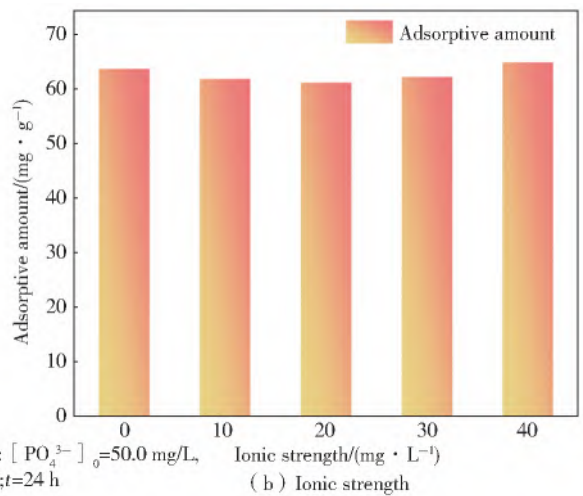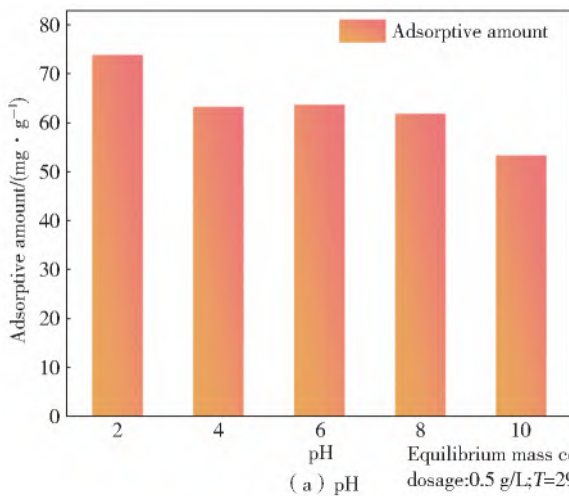
Fig. 8 Effects of initial solution pH and on PO_4^{3-} adsorption

Likewise，the effect of ionic strength on adsorption amount was also investigated (Fig. 8(b)). In a mixed system，the adsorptive amount showed negligible fluctuation although the mass concentration of NaCl increased to 40 mg/L. This suggested that MIL-101(Fe/Zr) could tolerate a high saline solution，and may hold good potential in removal of PO_4^{3-} from water.

3.3 Adsorption mechanism

As shown in Fig. 9, the XRD patterns of MIL-101(Fe/Zr) before and after adsorption had no obvious differences, but the diffraction intensity became a little weaker after adsorption. In the patterns, the lattice planes of (111) and (224) could be still clearly observed. This evidence suggested that phosphate had been attached to the surface of MIL-101(Fe/Zr) by the coordination interactions rather than the precipitation reactions. It is obvious that the phosphate species (PO_4^{3-}) strongly interacted with Fe-or Zr-containing active sites[33]. This could be explained why MIL-101(Fe/Zr) exhibited satisfactory adsorption performance.
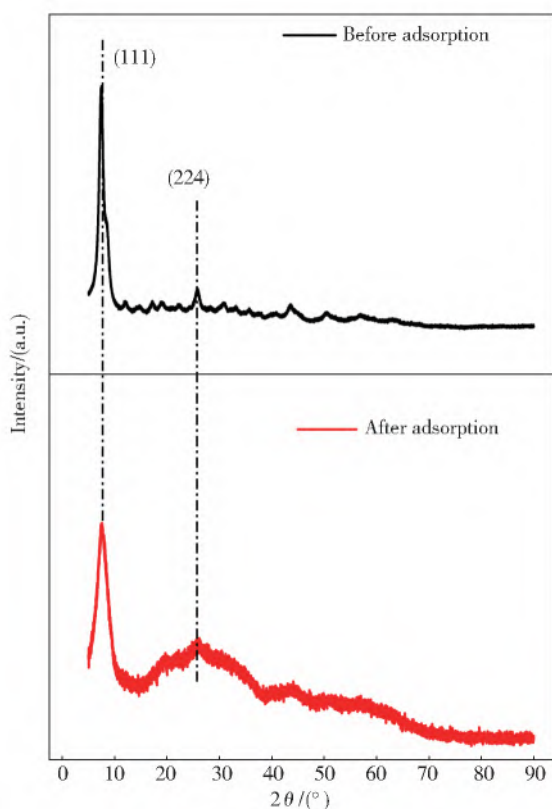
Fig. 9 XRD patterns of MIL-101(Fe/Zr) before and after adsorption of PO_4^{3-}

Besides, a fine observation of SEM images before and after adsorption, and determination of element species of MIL-101(Fe/Zr) after adsorption further verified the occurrence of adsorption behavior. In Fig. 10, the SEM image of MIL-101 (Fe/Zr) possessed a clear nanostructure before adsorption. When adsorbing phosphate, the surface became scaly. It can be inferred that PO_4^{3-} adsorption induced generation of this unique morphology in the interface. EDX spectra suggested the occurrence of the phosphorus element on the surface of used MIL-101(Fe/Zr), and it proved an adsorption behavior on the interface of MIL-101(Fe/Zr) and the solution[35].
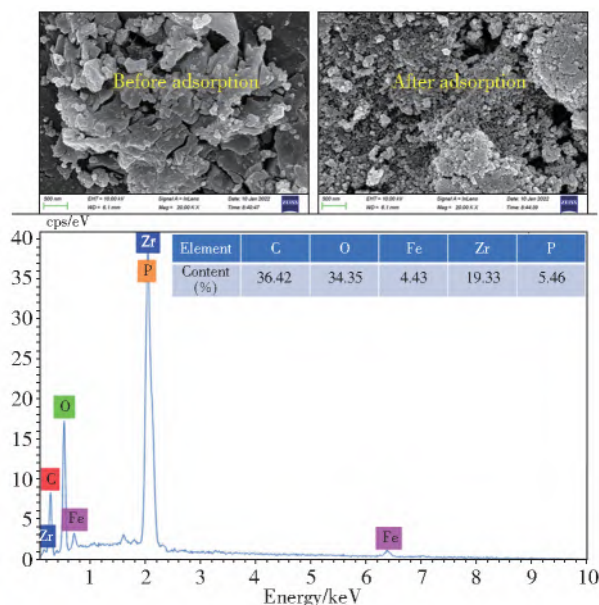
Fig. 10 SEM images of MIL-101(Fe/Zr) before and after adsorption of PO_4^{3-} and EDX spectrum of MIL-101(Fe/Zr) after adsorption

XPS spectra were used to identify the active sites of MIL-101(Fe/Zr), as shown in Fig. 11. A survey investigation and a high-resolution spectrum of P 2p clearly suggested the fact of successful attachment of PO_4^{3-} to the surface of MIL-101 (Fe/Zr) (Fig. 11(a) and (b)). XPS elementary analysis agreed well with the EDX determination. Generally, oxygen species could be deconvoluted into three types: lattice oxygen (O^{2-}), hydroxyl oxygen (HO^-), and water oxygen (H_2O). Fig. 11 (c) and (d) shows the change of oxygen species of MIL-101(Fe/Zr). The content of water oxygen almost kept unchanged with a fluctuation of 19.30% to 20.55%. The content of hydroxyl oxygen rose from 52.63% to 56.16%, while those of lattice oxygen diminished to 23.29% from 28.07%. These findings suggested that hydroxyl oxygen and lattice oxygen took part in adsorption reactions as active sites for phosphate species[36-37].

Moreover, the roles of metal elements in MIL-101(Fe/Zr) were also investigated. As displayed in Fig. 11(e) and (f), one can easily find that two characteristic peaks of Fe 2p moved to a high bind-

ing energy of 725. 6 and 711. 9 eV from 724. 5 and 711. 6 eV, respectively. For Zr 3d, one typical peak of Zr 3d exhibited a small shift to the high binding energy while the other one kept in the same site (Fig. 11(g) and (h)). These findings indicated that Fe-and Zr-based functional groups both served as active sites in adsorption of phosphate, and that the former might be dominated in the reaction[38].
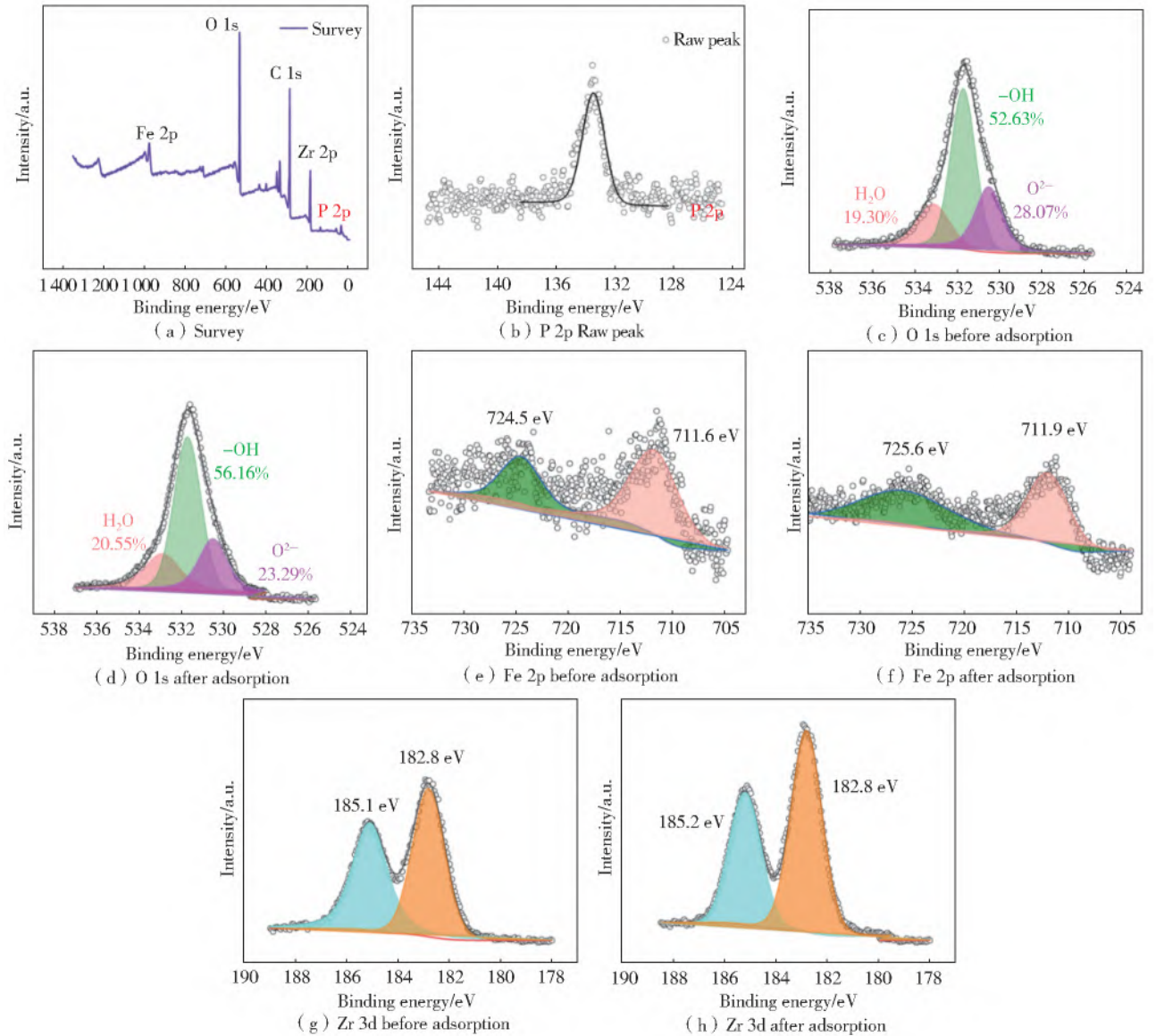
Fig. 11　XPS spectra of MIL-101(Fe/Zr) and MIL-101(Fe/Zr)-PO_4^{3-}: survey, P 2p, O 1s, Fe 2p, and Zr 3d

　　Totally, in one hand, phosphate may exist in H_3PO_4, $H_2PO_4^-$, HPO_4^{2-}, and PO_4^{3-} (negligible) in weak acidic solution. In the other hand, the unsaturated metal sites of MIL-101 (Fe/Zr) tended to form surface hydroxyls and then these hydroxyls would strongly interact with phosphate species. By ligand exchange reactions, the monodentate mononuclear or bidentate binuclear complex eventually formed in the surface of MIL-101 (Fe/Zr) (Fig. 12)[39].
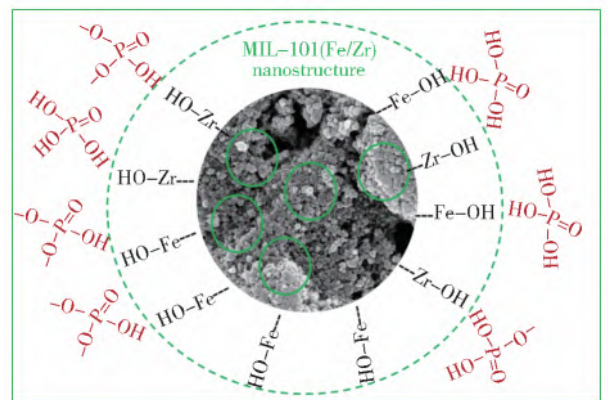
Fig. 12　Adsorption mechanism of PO_4^{3-} by MIL-101(Fe/Zr)

4　Conclusions

In summary, one novel type of bimetal-organic framework composite (denoted as MIL-101(Fe/Zr)) was prepared as an effective adsorbent for phosphate by a solvothermal method. This nanostructure shared a similar structure with MIL-101(Fe), implying the Zr atoms as a second metal were incorporated into the MIL-101(Fe) structure. The adsorption of PO_4^{3-} by MIL-101(Fe/Zr) conformed to the pseudo-second-order model and intraparticle diffusion model, and the Freundlich model well, suggesting a multiply-layer adsorption. It is suggested that such an adsorption belonged to multiply-layer adsorption. The adsorption capacity of MIL-101(Fe/Zr) was to be 66.00 mg/g, which is higher than those of other similar adsorbents. MIL-101 (Fe/Zr) performed well at a wide range of pH 2.0～10.0 and high ionic strength (0～40 mg/L NaCl). A characterization analysis indicated that PO_4^{3-} removal can be attributable to the complexation interaction between phosphate species and the adsorbent. Our findings may offer an alternative adsorbent for PO_4^{3-} recovery, and inspire design of other metal-based adsorbents.

References:

[1]　DE-BASHAN L E, BASHAN Y. Recent advances in removing phosphorus from wastewater and its future use as fertilizer (1997-2003)[J]. Water Research, 2004, 38: 4222-4246. DOI: 10. 1016/j. watres. 2004. 07. 014.

[2]　AKRAM M, GAO B, PAN J, et al. Enhanced removal of phosphate using pomegranate peel-modified nickel lanthanum hydroxide[J]. Science of the Total Environment, 2021, 809: 151-181. DOI: 10. 1016/j. scitotenv. 2021. 151181.

[3]　AZAM H M, ALAM S T, HASAN M, et al. Phosphorous in the environment: characteristics with distribution and effects, removal mechanisms, treatment technologies, and factors affecting recovery as minerals in natural and engineered systems[J]. Environmental Science and Pollution Research, 2019, 26: 20183-20207. DOI: 10. 1007/s11356-019-04732-y.

[4]　MORSE G K, BRETT S W, GUY J A, et al. Review: Phosphorus removal and recovery technologies[J]. Science of the Total Environment, 1998, 212: 69-81. DOI: 10. 1016/S0048-9697(97)00332-x.

[5]　JIAO G J, MA J L, LI Y C, et al. Recent advances and challenges on removal and recycling of phosphate from wastewater using biomass-derived adsorbents[J]. Chemosphere, 2021, 278: 130377. DOI: 10. 1016/j. chemosphere. 2021. 130377.

[6]　HUANG W, ZHANG Y, LI D. Adsorptive removal of phosphate from water using mesoporous materials: A review[J]. Journal of Environmental Management, 2017, 193: 470-482. DOI: 10. 1016/j. jenvman. 2017. 02. 030.

[7]　JIANG S, WANG J, QIAO S, et al. Phosphate recovery from aqueous solution through adsorption by magnesium modified multi-walled carbon nanotubes[J]. Science of the Total Environment, 2021, 796: 148907. DOI: 10. 1016/j. scitotenv. 2021. 148907.

[8]　WU B, LO I M C. Surface functional group engineering of CeO_2 particles for enhanced phosphate adsorption[J]. Environmental Science & Technology, 2020, 54: 4601-4608. DOI: 10. 1021/acs. est. 9b06812.

[9]　TRAN H N, YOU S J, HOSSEINI-BANDEGHARAEI A, et al. Mistakes and inconsistencies regarding adsorption of contaminants from aqueous solutions: A critical review[J]. Water Research, 2017, 120: 88-116. DOI: 10. 1016/j. watres. 2017. 04. 014.

[10]　CHEN Y, DU Y, LIU P, et al. Removal of ammonia emissions via reversible structural transformation in M(BDC) (M=Cu, Zn, Cd) metal-organic frameworks [J]. Environmental Science & Technology, 2020, 54: 3636-3642. DOI: 10. 1021/acs. est. 9b06866.

[11]　QIU S, ZHAO D, FENG Y, et al. Adsorption performance and mechanism of Ca-Al-LDHs prepared by oyster shell and pop can for phosphate from aqueous solutions[J]. Journal of Environmental Management, 2022, 303: 114235. DOI: 10. 1016/j. jenvman. 2021. 114235.

[12]　KHAN N A, HASAN Z, JHUNJ S H. Adsorptive removal of hazardous materials using metal-organic frameworks (MOFs): A review[J]. Journal of Hazardous Materials, 2013, 244-245: 444-456. DOI: 10. 1016/j. jhazmat. 2012. 11. 011.

[13]　RECEPOGLU Y K, GOREN A Y, OROOJI Y, et al. Carbonaceous materials for removal and recovery of phosphate species: Limitations, successes and future improvement[J]. Chemosphere, 2022, 287: 132177. DOI: 10. 1016/j. chemosphere. 2021. 132177.

[14]　ZHAO X, ZHANG N, YANG T, et al. Bimetallic metal-organic frameworks: Enhanced peroxidase-like activities for the self-activated cascade reaction[J]. ACS Appl Mater Interfaces, 2021, 13: 36106-36116. DOI: 10. 1021/acsami. 1c05615.

[15]　SHEN K, ZHANG L, CHEN X, et al. Ordered macro-

microporous metal-organic framework single crystals [J]. Science, 2018, 359: 206-210. DOI: 10.1126/science. aao. 3403.

[16] JANIAK C, VIETH J K. MOFs, MILs and more: Concepts, properties and applications for porous coordination networks (PCNs)[J]. New Journal of Chemistry, 2010, 34: 2366-2388. DOI: 10.1039/c0nj00275e.

[17] WANG W, XU B, PAN X, et al. Solvent-dependent adsorption-driven mechanism for MOFs-Based yolk-shell nanostructures[J]. Angewandte Chemie International Edition, 2021, 60: 7802-7808. DOI: 10.1002/anie. 202014895.

[18] BAI Y, DOU Y, XIE L H, et al. Zr-based metal-organic frameworks: Design, synthesis, structure, and applications[J]. Chemical Society Reviews, 2016, 45: 2327-2367. DOI: 10.1039/c5cs00837a.

[19] LI B, XU C, YU D, et al. Enhanced phosphate remediation of contaminated natural water by magnetic zeolitic imidazolate framework-8 @ engineering nanomaterials (ZIF8 @ ENMs)[J]. Colloid and Interface Science, 2022, 613: 71-83. DOI: 10.1016/j. jcis. 2022. 01. 003.

[20] YANG L, SHAN X, ZHAO Y, et al. Efficient phosphate capture of $Fe_3O_4/UiO-66-NH_2/CeO_2$ in wide pH spectrum[J]. Microporous and Mesoporous Materials, 2022, 331: 111653. DOI: 10.1016/j. micromeso. 2021. 111653.

[21] MOUMEN E, BAZZI L, HANKARI S EL. Metal-organic frameworks and their composites for the adsorption and sensing of phosphate[J]. Coordination Chemistry Reviews, 2022, 455: 214376. DOI: 10.1016/j. ccr. 2021. 214376.

[22] LIU M, HUANG Q, LI L, et al. Cerium-doped MIL-101-NH_2(Fe) as superior adsorbent for simultaneous capture of phosphate and As(V) from Yangzonghai coastal spring water[J]. Journal of Hazardous Materials, 2021, 423: 126981. DOI: 10.1016/j. jhazmat. 2021. 126981.

[23] WANG L, WEN X, LI J, et al. Roles of defects and linker exchange in phosphate adsorption on UiO-66 type metal organic frameworks: Influence of phosphate concentration[J]. Chemical Engineering Journal, 2021, 405: 126681. DOI: 10.1016/j. cej. 2020. 126681.

[24] SHANG Y, XU Q, GAO Z, et al. Enhanced phosphate removal from practical wastewater via in situ assembled dimension-engineered MOF@carbon heterostructures[J]. Chemical Engineering Journal, 2022, 428: 132536. DOI: 10.1016/j. cej. 2021. 132536.

[25] XUE H, HUANG X S, YIN Q, et al. Bimetallic cationic metal-organic frameworks for selective dye adsorption and effective $Cr_2O_7^{2-}$ removal[J]. Crystal Growth & Design, 2020, 20: 4861-4866. DOI: 10.1021/acs. cgd.
0c00239.

[26] KONG L, ZHANG J, WANG Y, et al. Bowknot-like Zr/La bimetallic organic frameworks for enhanced arsenate and phosphate removal: combined experimental and DFT studies[J]. Journal of Colloid and Interface Science, 2022, 10: 1001-1033. DOI: 10.1016/j. jcis. 2022. 01. 033.

[27] FANG L, ZENG W, XU L, et al. Green rusts as a new solution to sequester and stabilize phosphate in sediments under anoxic conditions and their implication for eutrophication control[J]. Chemical Engineering Journal, 2020, 388: 124198. DOI: 10.1016/j. cej. 2020. 124198.

[28] TAWEEKARN T, WONGNIRAMAIKUL W, CHOODUM A. Removal and recovery of phosphate using a novel calcium silicate hydrate composite starch aerogel [J]. Journal of Environmental Management, 2022, 301: 113923. DOI: 10.1016/j. jenvman. 2021. 113923.

[29] HUO J B, YU G. Hexacyanoferrate-modified polyvinyl alcohol/graphene oxide aerogel as an efficient and retrievable adsorbent for cesium[J]. Journal of Materials Science, 2022, 57: 351-365. DOI: 10.1007/s10853-021-06573-y.

[30] HUO J B, GUPTA K, LU C, et al. Recyclable high-affinity arsenate sorbents based on porous $Fe_2O_3/La_2O_2CO_3$ composites derived from Fe-La-C frameworks[J]. Colloids and Surfaces A: Physicochemical and Engineering Aspects, 2022, 585: 124018. DOI: 10.1016/j. colsurfa. 2019. 124018.

[31] HUANG L Z, ZHOU Y, ZHANG X, et al. Effect of structural properties of green rusts on phosphate fixation and implication for eutrophication remediation[J]. Separation and Purification Technology, 2021, 274: 119023. DOI: 10.1016/j. seppur. 2021. 119023.

[32] ALMANASSRA I W, KOCHKODAN V, SUBEH M, et al. Phosphate removal from synthetic and treated sewage effluent by carbide derive carbon[J]. Journal of Water Process Engineering, 2020, 36: 101323. DOI: 10.1016/j. jwpe. 2020. 101323.

[33] FENG L, ZHANG Q, JI F, et al. Phosphate removal performances of layered double hydroxides (LDH) embedded polyvinyl alcohol / lanthanum alginate hydrogels[J]. Chemical Engineering Journal, 2022, 430: 132754. DOI: 10.1016/j. cej. 2021. 132754.

[34] QING Z, WANG L, LIU X, et al. Simply synthesized sodium alginate/zirconium hydrogel as adsorbent for phosphate adsorption from aqueous solution: Performance and mechanisms[J]. Chemosphere, 2021, 133103. DOI: 10.1016/j. chemosphere. 2021. 133103.

sediment ecological risk assessment. Shahe Reservoir，Miyun Reservoir，Guanting Reservoir and Yuqiao Reservoir are selected as the main research objects because of heavy metal pollution and ecological effects in reservoirs. The data on the mass fraction and toxicology of heavy metals in reservoir sediments were obtained from published articles and journals. Through the analysis of distribution characteristics and correlation analysis，the distribution characteristics and pollution sources of heavy metal sediments were judged. The geological accumulation index and potential ecological risk index were used to evaluate the ecological risk level of heavy metal sediments. Finally，the species sensitivity index was used to evaluate the proportion of potentially harmful species in heavy metal sediments. The distribution characteristics and correlation analysis results show that the distribution of heavy metals in the sediments of the four typical reservoirs are similar to some extent，and the mass fraction of heavy metals are comparable. The distribution of heavy metal deposits in reservoirs of Haihe River basin is similar to some extent，and the mass fraction of heavy metal in sediments may be affected by industrialization. The results of ecological risk analysis showed that As was the most polluted heavy metal in the sediments of the four reservoirs. The ecological risk grade of Shahe Reservoir，Miyun Reservoir and Yuqiao Reservoir is low，but for Guanting Reservoir is medium. Species sensitivity distribution showed that different heavy metals had different mass fraction of harmful mass（HC_5）to 5% of benthic species. The average harmful species proportion（PAF）of heavy metals in the sediments of four typical reservoirs from high to low is Zn(97.5%)>Cu(97.1%)>Cr(96.6%)>Zn(92.2%)>Pb（91.8%）>Ni(90.8%). These results indicate that the six heavy metals in sediment may have certain effects on the survival of more than 90% of the benthic organisms in the reservoir. The overall results show that the mass fraction of heavy metals in the sediment a reservoir is relatively low，and the ecological risk level is good，but the impact of heavy metals in the sediment on the benthos of the reservoir cannot be ignored. The research results are helpful to understand the ecological risk of heavy metals in reservoir sediments and provide the basis for reservoir ecological management.

Key words：reservoir；heavy metals；sediment；ecological risk；species sensitivity distribution

［35］ WANG Z，XIA D，CUI S，et al. A high-capacity nano-cellulose aerogel uniformly immobilized with a high loading of nano-La(OH)₃ for phosphate removal[J]. Chemical Engineering Journal，2022，433：134439. DOI：10.1016/j.cej.2021.134439.

［36］ WAN J，WU B，LO I M C. Development of Fe₀/Fe₃O₄ composites with tunable properties facilitated by Fe₂⁺ for phosphate removal from river water[J]. Chemical Engineering Journal，2020，388：124242. DOI：10.1016/j.cej.2020.124242.

［37］ SHAN X，YANG L，ZHAO Y，et al. Biochar/Mg-Al spinel carboxymethyl cellulose-La hydrogels with cationic polymeric layers for selective phosphate capture [J]. Journal of Colloid and Interface Science，2022，606：736-747. DOI：10.1016/j.jcis.2021.08.078.

［38］ DU Y，WANG X，NIE G，et al. Enhanced phosphate removal by using La-Zr binary metal oxide nanoparticles confined in millimeter-sized anion exchanger[J]. Journal of Colloid and Interface Science，2020，580：234-244. DOI：10.1016/j.jcis.2020.07.011.

［39］ ZHANG B，XU L，ZHAO Z，et al. Enhanced phosphate removal by nano-lanthanum hydroxide embedded silica aerogel composites：Superior performance and insights into specific adsorption mechanism[J]. Separation and Purification Technology，2022，285：120365. DOI：10.1016/j.seppur.2021.120365.